AIAA JOURNAL
Vol. 56, No. 4, April 2018

Density Fluctuations Measurement by Rayleigh Scattering Using a Single Photomultiplier

Bertrand Mercier*
Central School of Lyon, 69134 Écully, France
Thomas Castelain†
Claude Bernard University Lyon 1, 69134 Écully, France
and
Emmanuel Jondeau‡ and Christophe Bailly§
Central School of Lyon, 69134 Écully, France

DOI: 10.2514/1.J056507

Rayleigh scattering provides a direct nonintrusive method for density measurement, which is of particular interest in aeroacoustics. However, two major concerns arise linked to the use of photomultipliers. First, the detection of photon flux is corrupted by the presence of dust particles in the flow. An original signal processing is proposed in this study to remove their signatures. Second, the random arrival of photons on a photomultiplier induces shot noise, which can be partly removed by using two photomultipliers. It is shown in this study that a single photomultiplier combined with suitable processing can also be used to remove shot noise. Both approaches are compared for the case of a compressible subsonic jet exhausting in an anechoic wind tunnel.

Nomenclature

c	=	speed of light, $\mathrm{m}\cdot\mathrm{s}^{-1}$
d	=	beam diameter, m
$\mathrm{d}\sigma/\mathrm{d}\Omega$	=	differential scattering cross section, $\mathrm{m}^2\cdot\mathrm{sr}^{-1}$
$\mathrm{d}\sigma/\mathrm{d}\Omega^{\perp}$	=	differential scattering cross section at 90 deg, $\mathrm{m}^2\cdot\mathrm{sr}^{-1}$
$\mathrm{d}\Omega$	=	solid angle of light collectors, sr
f	=	focal length, m
f_s	=	sampling frequency, Hz
h	=	Planck's constant, $\mathrm{kg}\cdot\mathrm{m}^2\cdot\mathrm{s}^{-1}$
I	=	laser intensity, $\mathrm{W}\cdot\mathrm{m}^{-2}$
k	=	proportionality constant, $\mathrm{kg}\cdot\mathrm{s}\cdot\mathrm{m}^{-3}$
$\mathcal{M}$	=	molecular mass, $\mathrm{kg}\cdot\mathrm{mol}^{-1}$
m	=	generic index
N	=	count rate
$\mathcal{N}$	=	numeric density, m^{-3}
N_A	=	Avogadro constant, mol^{-1}
n	=	Poisson distribution parameter
P_s^i	=	scattered power by individual molecules, W
P_s	=	total scattered power, W
Q_E	=	quantum efficiency of photomultiplier
t_s	=	dust signature width, s
V	=	velocity, $\mathrm{m}\cdot\mathrm{s}^{-1}$
V_{sc}	=	probed volume, m^3
Δf	=	frequency resolution, Hz
σ	=	standard deviation
λ	=	laser wavelength
ρ	=	density, $\mathrm{kg}\cdot\mathrm{m}^{-3}$
τ	=	pulse pair resolution, s
ϕ	=	phase, rad
Φ	=	photon arrival rate, s^{-1}
ψ	=	polarization angle, rad
$\bar{\ }$	=	time average

Subscripts

amb	=	quantity related to ambient
d	=	quantity related to a detected quantity
j	=	quantity in the jet potential core
SN	=	shot noise
0	=	total quantity
1	=	quantity related to the collector 1
2	=	quantity related to the collector 2

Superscripts

$'$	=	fluctuating part
i, j	=	generic indexes

Received 7 July 2017; revision received 27 October 2017; accepted for publication 21 November 2017; published online 28 December 2017.

*Ph.D. Student, LMFA UMR CNRS 5509; bertrand.mercier@doctorant.ec-lyon.fr.
†Assistant Professor, LMFA UMR CNRS 5509.
‡Research Engineer, LMFA UMR CNRS 5509.
§Professor, LMFA UMR CNRS 5509. Senior Member AIAA.

I. Introduction

A. Context

THE development of nonintrusive and quantitative techniques for the measurement of high-speed compressible flow properties is a major concern for aeroacoustics purposes. Rayleigh scattering-based methods unambiguously meet these requirements because they give access to time-resolved flow properties such as the density, temperature, and velocity, without using intrusive probe or flow seeding. These techniques rest upon the analysis of the laser light scattered by the fluid molecules that constitute the region of interest in the flow. The intensity of the scattered light is related to the density [1], which led to pioneering applications in aeroacoustics by Seasholtz and Panda [2], Panda and Seasholtz [3], and Panda et al. [4–6]. Other properties of the scattered light are related to further physical parameters. The broadening of the spectrum provides information about temperature, and the local flow velocity is related to the central frequency shift due to the Doppler effect [7–9].

The present effort is part of the development of such a method for the measurement of density fluctuations at high frequency in the anechoic wind tunnel of the Centre for Acoustics in École Centrale de Lyon. Original approaches about the light intensity measurement, the signal processing for cleaning signals from corrupted data, and the calculation of density fluctuations are proposed. In particular, it is demonstrated that density fluctuations can be measured from a single photosensor without the usual limitations regarding shot noise.

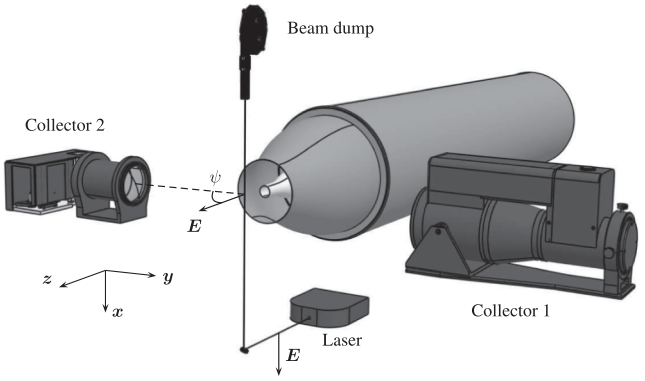

Fig. 1 Sketch of the experimental setup.

B. Rayleigh Scattering Theory

Light scattering from particles of small dimension in comparison to the incident light wave length λ is related to the Rayleigh scattering theory. This is an elastic scattering process [10], meaning that no energy is lost, even though the scattered light spectrum is broader than that of the incident light. This is the result of the Doppler effect involved by the individual motion of molecules due to thermal agitation and by the bulk motion representative of the local flow velocity [10,11].

Light is scattered by molecules in all directions, but for practical reasons, only a small fraction can be collected into a solid angle $\mathrm{d}\Omega$, depending on the size of the light collector device. The ability for a given particle to scatter light is determined by its differential scattering cross section $\partial\sigma/\partial\Omega$, which depends on the direction of observation. For spherical particles, this quantity is only a function of the angle ψ between the electric field vector $\boldsymbol{E}$ of the incident light and the direction of observation; refer to Fig. 1. For a linearly polarized laser light, $\partial\sigma/\partial\Omega$ can be deduced from the differential scattering cross section $\partial\sigma/\partial\Omega^{\perp}$ at $\psi = 90°$:

$$\frac{\partial\sigma}{\partial\Omega} = \frac{\partial\sigma^{\perp}}{\partial\Omega}\sin^2(\psi) \tag{1}$$

The power of the light scattered P_s^i by a single molecule undergoing a laser beam of intensity I, and collected into $\mathrm{d}\Omega$ at an angle ψ, is given by

$$P_s^i = \frac{\partial\sigma^{\perp}}{\partial\Omega}\mathrm{d}\Omega\sin^2(\psi)I \tag{2}$$

In fluid mechanics, the particles of interest are the molecules constituting the gas mixture, namely dinitrogen and dioxygen. To account for the different types of molecules, $\partial\sigma/\partial\Omega$ is calculated as an average of the differential scattering cross sections of all species, weighted by their concentrations. The number of molecules per unit of volume $\mathcal{N}$ can be determined from Avogadro's constant N_A, the molecular mass $\mathcal{M}$, and the density ρ:

$$\mathcal{N} = \frac{\rho N_A}{\mathcal{M}} \tag{3}$$

Finally, the power of light scattered by all the molecules contained inside a probe volume V_{sc} is equal to the sum of the power scattered by all the individual molecules:

$$P_s = \frac{\rho N_A}{\mathcal{M}}V_{\mathrm{sc}}\frac{\partial\sigma^{\perp}}{\partial\Omega}\mathrm{d}\Omega\sin^2(\psi)I \tag{4}$$

This relation shows that, for a given gas, laser, and light collector size and position, the scattered power is proportional to the density. The goal is thus to measure P_s to determine the local density of air. However, air is also made of low-concentrated larger particles such as dust particles, whose contribution to the scattered power is larger than molecular contribution by many orders of magnitude. As a consequence, the studied gas must be kept as free as possible from any particle larger than the molecular scale.

C. Facilities and Equipment Description

The Rayleigh scattering-based measurement system is operated to measure jet flow properties in an anechoic wind tunnel. Even if the primary airstream was free of dust particles, entrainment of particle-laden ambient air would contaminate Rayleigh scattering measurements. To mitigate this problem, the two air supplies of the wind tunnel, a high-pressure compressor and a high-flow-rate fan, are equipped with high-efficiency filters. These filters are capable of removing almost all the particles of diameter larger than a few tenths of a micrometer [6]. The compressor feeds a convergent nozzle of 38 mm in diameter at a Mach number up to 1.56, whereas the low-pressure supply is connected to a secondary coaxial nozzle of diameter 200 mm. The flow from the secondary nozzle is exhausted at low speed, typically $10\ \mathrm{m}\cdot\mathrm{s}^{-1}$, to generate a clean environment for the inner high-speed jet to develop in, and without drastically affecting its properties with respect to a single jet configuration. In addition, an air dryer is mounted downstream of the compressor to limit the amount of water vapor that is likely to condensate due to the air expansion at the nozzle exit.

As shown in Fig. 1, the measurement system relies on the light emitted by a $\lambda = 532$ nm continuous 5 W laser. The light collection devices consist of two independent devices of focal length $f_1 = 750$ mm and aperture $f_1/5$, and $f_2 = 450$ mm and $f_2/4.3$, respectively. They are mounted in front of each other and collect the light scattered from a cylindrical probed volume of approximately 1 mm in diameter and 0.3 mm in height. In each collector, the light is focused onto a Hamamatsu H7422-P40 photomultiplier, which converts the detection of photons in pulses of electric charges. For the typical detection rate considered in the flowing, the signal consists of discrete pulses indicating each detection.

A new technique for photon counting is implemented in the present Rayleigh scattering bench to increase the linearity of the measure [Eq. (4)]. The output signal of the photomultiplier is directly digitized by a high-speed data acquisition system. The digitizer National Instrument NI-5160 is chosen for its maximum sampling frequency of 2.5 GHz and its memory of 2 GB. Considering the maximum bandwidth of the card, the sampling frequency has been limited to 1.25 GHz, allowing 0.86 s of continuous record for one channel or 0.43 s for two channels.

The laser, beam dump, and collecting optics are mounted on a single rigid frame stood on a two-axis traverse system to make attainable any location of interest in and near the jet flow. Unless otherwise noted, results shown in next sections are recorded at the location of the fluctuation peak in the mixing layer and three diameters downstream of the nozzle exit.

II. Scattered Power and Photon Flux Estimation

A. Principle of Photon Counting Techniques

The power of the collected scattered light can be estimated from Eq. (4) according to the numerical values provided in Table 1,

Table 1 Parameter values of the Rayleigh scattering bench

Parameter	Value
λ	532 nm
V_{sc}	$2.3\times10^{-10}\ \mathrm{m}^3$
I	$6.4\times10^{6}\ \mathrm{W}\cdot\mathrm{m}^{-2}$
$\partial\sigma/\partial\Omega$	$5.9\times10^{-32}\ \mathrm{m}^2\cdot\mathrm{sr}^{-1}$
$N_A/\mathcal{M}$	$2.1\times10^{25}\ \mathrm{kg}^{-1}$
$1/(hc)$	$5.0\times10^{24}\ \mathrm{J}^{-1}\cdot\mathrm{m}^{-1}$
ψ	$\pi/2$ rad
$\mathrm{d}\Omega_1$	3.1×10^{-2} sr
$\mathrm{d}\Omega_2$	4.4×10^{-2} sr
Q_E	0.3

representative of the present setup. That provides $P_s = 6.8 \times 10^{-11}$ W for the smallest collecting device in air of density 1.2 kg $\cdot$ m^{-3}, a too-small value to be directly measured. A convenient approach to measure such a light power P_s is to convert it into a flux of photons of energy hc/λ, where h is Planck's constant, and c the speed of light. By introducing a quantum efficiency Q_E that equals the probability for a collected photon to be detected by the photomultiplier, Eq. (5) helps in determining the flux of detected photons Φ_d:

$$\Phi_d = \underbrace{Q_E(\lambda/hc)(N_A/\mathcal{M})(\partial\sigma/\partial\Omega)^{\perp}\mathrm{d}\Omega V_{\mathrm{sc}}\sin^2(\psi)I}_{=k}\rho \tag{5}$$

that is the rate of arrival of photons that produces electric pulses on the photomultiplier output signal. For a given experimental setup, the term underbrace is a calibration constant denoted k, giving

$$\rho = \Phi_d/k \tag{6}$$

The measurements obtained from photon counting are, however, affected by an intrinsic uncertainty called shot noise, resulting of the randomness of photon arrivals on the sensor. Even for a constant light flux, the number of incoming photons during a certain amount of time randomly varies. The probability of detecting a photon during an interval of time dt follows a Poisson distribution of parameter $\Phi_d dt$. The variance of the number N of photons counted during dt in repeated measurements is equal to the expected value $\bar{N} = \Phi_d dt$. The standard deviation of the shot noise σ_{SN} is thus

$$\sigma_{\mathrm{SN}} = \sqrt{\mathrm{Var}(N)} = \bar{N}^{1/2} \tag{7}$$

and the signal-to-noise ratio (SNR) is given by

$$\mathrm{SNR} = \frac{\bar{N}}{\sigma_{\mathrm{SN}}} = \bar{N}^{1/2} = (\Phi_d dt)^{1/2} \tag{8}$$

To increase this signal-to-noise ratio, the flux of photons must be maximized. However, counting two consecutive photons is impossible if their times of arrival are separated by a delay smaller than the pulse pair resolution τ, which corresponds either to a time constant associated with the counter or with the photomultiplier. This phenomenon is known as the pileup effect. The probability to count a photon is therefore the probability that no photon is detected during τ. From Poisson's law, the probability for detecting n photons during dt is

$$p(n, dt) = \frac{(\Phi_d dt)^n}{n!} e^{-\Phi_d dt} \tag{9}$$

thus, the probability of counting no photon during τ is $p(0, \tau) = e^{-\Phi_d \tau}$. This probability decreases when τ and Φ_d increase. Because Φ_d should be kept as high as possible, τ should be as short as possible. Nevertheless, even with these precautions taken, the counted flux Φ is smaller than the detected flux:

$$\Phi = \Phi_d e^{-\Phi_d \tau} \tag{10}$$

B. Advantage of the Present Method for Photon Counting

A traditional commercial system counter such as the SRS SR-400 with $\tau = 5$ ns is limited to very short records. On the contrary, the Hamamatsu C9744 allows longer records, but $\tau = 25$ ns. In the present bench, the output signal of the photomultiplier is digitized during either 0.86 s in a single-channel configuration or 0.43 s in a two-channel configuration, and the photon counting is obtained throughout a software processing. An example signal is shown in Fig. 2. The signal contains peaks that demarcate well from the noise floor. A fixed threshold of value determined from the distribution of the peak amplitude is therefore suitable for discriminating the peaks associated with photon from electronic noise. The result of the processing is made of two long tables containing the arrival time and the amplitude of each peak. A time history of the count rate N along successive time bin of width δt is then calculated by counting the photons arrived in each bin. The photon flux is then obtained by calculating $\Phi(t) = N(t)/\delta t$, and the density is therefore sampled at a frequency $f_s = 1/\delta t$. The main benefit of this method for acquiring signals is its low value of τ, estimated to be lower than 2 ns. Furthermore, the sampling frequency can be freely chosen during the postprocessing step.

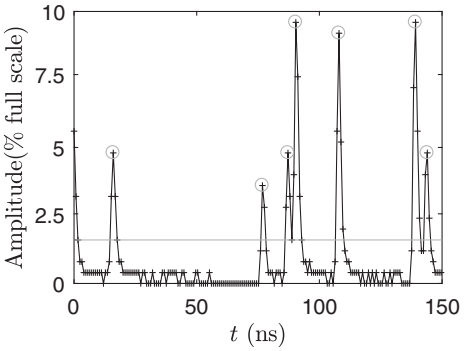

Fig. 2 Sample of the photomultiplier signal. ○ detected photons; — detection threshold.

C. Pileup Correction

The flux Φ_d introduced in Eq. (5) is at first unknown because counting ends up with Φ. Equation (10) must therefore be inverted by using the Lambert W function, for instance. The pileup correction can also be achieved through the Taylor expansion of Φ:

$$\Phi = \Phi_d e^{-\Phi_d \tau} \simeq \Phi_d - \tau\Phi_d^2 \tag{11}$$

as $\Phi_d \tau$ tends to zero. By noting that the right-hand side of Eq. (11) is also the Taylor expansion of

$$\frac{\Phi_d}{1 + \tau\Phi_d} \simeq \Phi_d(1 - \tau\Phi_d) \tag{12}$$

and that the term $\Phi_d \tau$ is expected to be small, the detected flux Φ_d can be estimated as

$$\Phi_d \simeq \frac{\Phi}{1 - \tau\Phi} \tag{13}$$

The number of detected photons per time bin is thus

$$N_d \simeq \frac{N}{1 - \tau N f_s} \tag{14}$$

As an illustration, this approximation leads to an error of 0.44% for a typical value of $\Phi_d \tau = 0.1$.

D. Flux Components

An example of time history of the count rate of photon in time bin of 5 μs is shown in Fig. 3. Two components can be observed in this signal: a contribution made of high positive peaks and a contribution distributed symmetrically around the average value. The high value peaks result from the detection of dust particles passing across the probed volume. They correspond to corrupted parts of the signal that do not contain any information about the density and should therefore be removed. The random part centered around the average is made of density fluctuations and of shot noise. As mentioned in Sec. II.A, the shot noise is well defined, and its standard deviation σ_{SN} can be calculated from Eq. (7). Here, $\bar{N} \simeq 220$ photons during 5 μs; thus, $\sigma_{\mathrm{SN}} \simeq 15$ photons/5 μs, which is approximately 7% of the average value. In most cases requiring fast sampling rates, such as in this

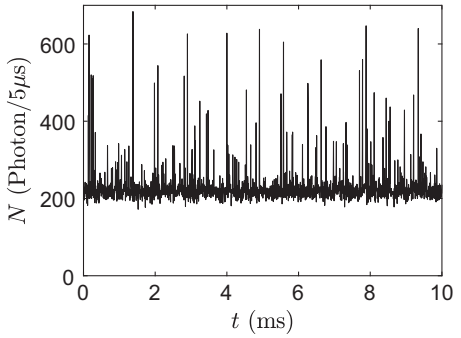

Fig. 3 Time history of the photon count rate for a sampling frequency of 200 kHz.

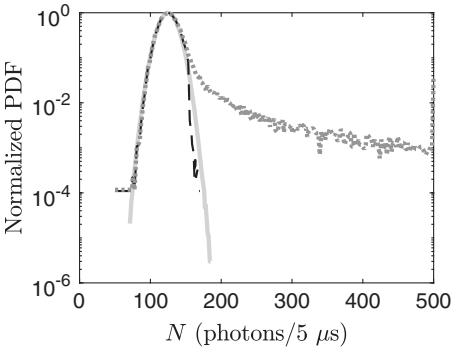

Fig. 4 Normalized probability density function of a signal sampled at 500 kHz. ⋯ raw signal; – – – cleaned signal; — Gaussian distribution.

study, density fluctuations are smaller than the shot noise contribution and much smaller than spike contribution.

E. Removal of Particle Signatures in Time Signals

A simple method to reduce the effect of the particle signatures in the signal is proposed in [6] for measurements in a heated boundary layer. The principle consists of replacing time history data larger than α times the standard deviation of the raw signal by the average count rate. In other words, for the ith point of the signal, if $N_d^i > \alpha\sigma_{N_d}$, then $N_d^i = \overline{N_d}$. The constant α is set according to the measured fluxes.

This cleaning method has, however, three potential inconveniences for jet flows. First, the corrupted points are replaced by the average value of the signal that contains those corrupted points; thus, the average value of the flux is overestimated. This effect remains small as long as the concentration in particles is low. Second, the standard deviation of the signal largely depends upon the number of spikes. This might not be a problem in a flow that contains a constant concentration in particles where α should be kept constant. If the concentration changes in space or in time, the threshold should be changed accordingly to an unknown value. This problem is of particular importance for the present experimental setup because the high-speed inner jet and the low-speed coflow are independently powered and thus do not contain the same dust concentration. Moreover, at high speed, residual water vapor contained in the air tends to condensate, and droplets emerge in different regions of the flow. The last difficulty is related to the use of two probes to compute two-point density correlations. If the probe volumes are located close to each other, the probes are likely to detect the same dust particles. Because the corrupted data points are replaced by a constant value, the correlation coefficient between these signals is overestimated.

An alternative cleaning method is proposed in this study to deal with these three points more accurately. The average flux and the standard deviation are estimated without bias induced by the presence of spikes. The probability density function of $N_d(t)$ is assumed to be a Gaussian because the shot noise dominates the fluctuations of $N_d(t)$ and because the difference between Poisson and Gaussian distributions is negligible for values of $\Phi_d dt$ greater than 12. In addition, the contribution of spikes is likely to only degrade the region of high count rates in the distribution. An example of count rate distribution is shown in Fig. 4, together with a fitted Gaussian distribution determined as follows. Because the high count rate region of this distribution is biased by the contribution of spikes due to the particles crossing the probe volume, only the low count rate part of the distribution is reliable and used to estimate the parameters of the Gaussian law. The mean value, that is the average count rate $\overline{N_d}$, is determined by the peak of the count rate distribution, $\overline{N_d} \simeq 125$ in the example of Fig. 4. The standard deviation is given by the half-width on the low count rate side. The part of the distribution that deviates from the fitted Gaussian distribution is then corrected. All bins of count rate higher than a threshold arbitrarily defined to be $\overline{N_d} + 3\sigma_{N_d}$ are replaced by a random number computed from a normal distribution $\mathrm{Nor}(\overline{N_d}, \sigma^2_{N_d})$. As a consequence, the corrections of signals from two different sensors are not correlated. The result of this cleaning process is plotted in dashed line in Fig. 4. The corrected signal distribution is much closer to a Gaussian distribution than the raw data.

This method can be optimized by choosing a sampling frequency ensuring that the width of spikes t_s is independent of the flow velocity. For a beam diameter d and a local average velocity V, the maximum spike width t_s associated with the time of flight of a particle within the probed volume is $t_s = V/d$. If the sampling frequency is too low, the spike is made of only one point, but some noncorrupted signal can be hidden, and so the spike should be discretized by a few points to reduce the corrupted proportion of signal. Conversely, if the spike is too much discretized, the sharp rise will not be detected by the cleaning process, and corrupted bins may remain. These two opposite cases are illustrated in Fig. 5 with the same spike sampled at the nominal frequency of 500, 125, and 2000 kHz. For the comparison, the average value of the signals $\overline{N_d}$ are subtracted, and their amplitudes are normalized by $\overline{N_d}^{1/2}$, that is close to the expected shot noise standard deviation. Sampling spikes by 3–10 bins with an optimal value fixed to 4 has been found to be a good compromise. Thus, f_s is chosen to be

$$f_s = 4\frac{d}{V} \tag{15}$$

The determination of f_s requires an estimate of the mean velocity that can be either measured by another mean or modeled according to the flow features.

The two methods can be assessed by comparing σ_{N_d} against $\sqrt{\overline{N_d}}$. These quantities should be equal if the density fluctuations contribution is insignificant with respect to the shot noise. In a Mach 0.9 cold jet for the present study, and the sampling frequency calculated from Eq. (15), the influence of the density fluctuations on σ_{N_d} is an increment of a few percent with a maximum of 7% in the mixing layer. Therefore, differences between $\overline{N_d}$ and σ_{N_d} larger than a few percent indicate defaults in the cleaning process. In Fig. 6, the excess of fluctuations is represented against the radial location at three diameters downstream of the nozzle exit. This quantity is provided for the raw signals of the two light collectors, the signals cleaned with the present method, and with the method proposed in [6]

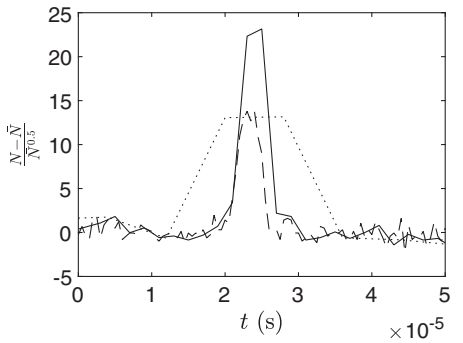

Fig. 5 Normalized count rate of a given spike, sampled at — 500 kHz; ⋯ 125 kHz; – – – 2 MHz.

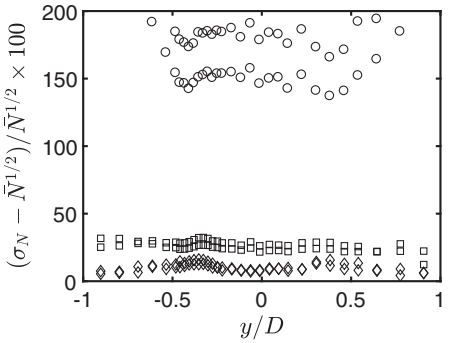

Fig. 6 Normalized excess of fluctuations of $N(t)$ from the two collectors: ○ no cleaning, □ [6], ◇ present method.

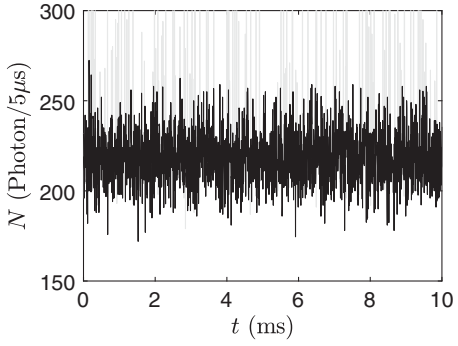

Fig. 7 Time history of the photon count rate sampled at 200 kHz, after treatment. In gray, the original signal as displayed in Fig. 3.

with a threshold adapted to the present study. Namely, if $N_d^i > \overline{N_d} + 3\sigma_{N_d}$, then $N_d^i = \overline{N_d}$. The gain brought by the present software cleaning is undeniable. The excess of fluctuations calculated from the signal cleaned with the present method is very little dependent upon the light collector and thus upon the average light flux, which differs from each collector. A dependency would be translated by two shifted sets of results such as for the simpler method. An example is shown in Fig. 7 for the signal presented in Fig. 3. The cleaning process replaced 5% of the original signal, and the resulting signal seems well preserved and clean of spikes likely to change the fluctuations associated features of the signal. The present method requires small density fluctuations in comparison with shot noise, but this hypothesis is satisfied for most of the usual turbulent flows, including jets.

F. Calibration of the Measurement System

Equation (6) provides a linear relation between the photon flux and the density, if the collected light is directly linked to a Rayleigh scattering. In real experimental conditions, there is inevitably some stray light in the environment of the light collector. This light mostly originates from the reflections of the laser beam on optic devices and on the beam dump. Some light also leaks from the outdoor of the anechoic room. This stray light represents a constant flux b that adds up the Rayleigh scattering associated light such that

$$\Phi_d = k\rho + b \tag{16}$$

Coefficients k and b are determined through a calibration method proposed in [12], which consists of placing the probed volume in the potential core of a jet. By measuring the total temperature of the flow T_0 as well as the ambient and the total pressures P_{amb} and P_0, the density in the potential core ρ_j can then be determined:

$$\rho_j = \frac{P_0}{rT_0}\left(\frac{P_0}{P_{\text{amb}}}\right)^{-(1/\gamma)} \tag{17}$$

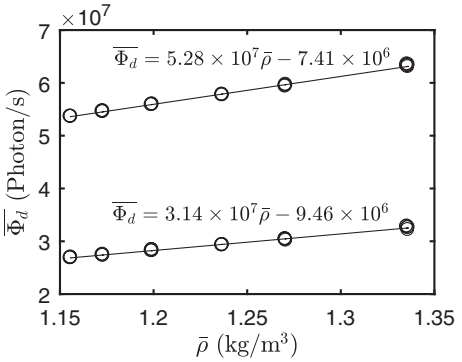

Fig. 8 Calibration curves of the dual light collector devices.

for an isentropic flow, where r is the gas constant, and γ is the ratio of specific heats of air. The mean photon flux has been measured for various flow Mach number, and the results are shown in Fig. 8. Coefficients k and b are estimated by computing the best fit line for the data in symbols. The proportionality coefficient k_1 and k_2 of the two light collectors are found to be $k_1 = 3.14 \times 10^7$ photons $\cdot$ m$^3 \cdot$ kg$^{-1} \cdot$ s^{-1} and $k_2 = 5.28 \times 10^7$ photons $\cdot$ m$^3 \cdot$ kg$^{-1} \cdot$ s^{-1}. For comparison, an estimation can be obtained from Eq. (5) that predicts $k_1 = 4.5 \times 10^7$ photons $\cdot$ m$^3 \cdot$ kg$^{-1} \cdot$ s^{-1} and $k_2 = 6.4 \times 10^7$ photons $\cdot$ m$^3 \cdot$ kg$^{-1} \cdot$ s^{-1}, which is in good agreement with the real values.

III. Application to Density Measurements

A. Time-Averaged Density

The mean density can be determined from the mean photon flux and the use of Eq. (16), as illustrated in Fig. 9. The density is averaged from 2.4 s of record from two photomultipliers (PMs), which corresponds to about 2×10^8 counted photons, leading to an SNR in the order of 10^4 according to Eq. (8). Uncertainties due to shot noise are therefore insignificant. The measured density is found close to the ambient density ρ_{amb} outside the jet and reaches the expected density ρ_j given by Eq. (17) in the potential core.

B. Density Fluctuations

As explained previously, density fluctuations are significantly smaller than those induced by shot noise, but the well-known properties of shot noise can be used to extract them.

1. *Shot Noise Contribution*

In flux signals, the shot noise is statistically independent of the density fluctuations ρ'. Thus, the variance of both signals can be added such that

$$\text{Var}(\Phi_d) = \text{Var}(\text{SN}) + \text{Var}(k\rho') \tag{18}$$

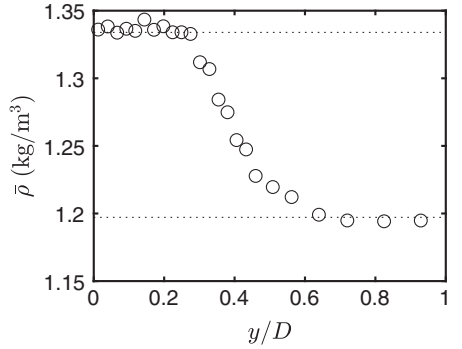

Fig. 9 Measured radial profile of the density in a Mach 0.9 cold jet at $z = 3D$.

Because the variance of the shot noise is equal to the average flux, one has

$$\sigma^2_{\Phi_d} = \overline{\Phi_d} + k^2\sigma^2_{\rho'} \tag{19}$$

and consequently,

$$\sigma_{\rho'} = \frac{\sqrt{\sigma^2_{\Phi_d} - \overline{\Phi_d}}}{k} \tag{20}$$

The rms density fluctuations can be deduced from this relation, but the accuracy of the results will greatly depend upon the ability to estimate the flux fluctuations. As shown in Sec. II.E, this estimation fails as soon as the flow is not completely free of dust particles and cannot be employed in realistic configurations.

2. *Two-Photomultiplier Cross-Spectrum*

A solution to get round of the difficulty to estimate shot noise contribution for density fluctuations measurement is proposed in [3]. The cross-spectrum of signals is obtained from two independent photomultipliers that probe the same flow volume. The fluctuations induced by the density are coherent on each signal but not the shot noise contribution. The two signals N_1 and N_2 are divided into m segments of length determined from the wanted frequency resolution Δf, and that can overlap. They are denoted N_1^j and N_2^j with $j = 1, 2, 3, \ldots, m$. The Fourier transform of each segment $F_{N_1^j}(f)$ and $F_{N_2^j}(f)$ is decomposed into a shot noise and an aerodynamic contribution:

$$F_{N_1^j}(f) = F_{N_{1A}^j} + F_{N_{1SN}^j} \qquad F_{N_2^j}(f) = F_{N_{2A}^j} + F_{N_{2SN}^j} \tag{21}$$

The one-sided power density spectrum $P_{N1N2}(f)$ is then calculated:

$$P_{N1N2}(f) = \frac{2}{m}\sum_{j=0}^{m-1} F_{N_1^j}(f)F^*_{N_2^j}(f) \tag{22}$$

where $*$ denotes the complex conjugate. It yields

$$P_{N1N2}(f) = \frac{2}{m}\sum_{j=0}^{m-1} \underbrace{F_{N_{1SN}^j}F^*_{N_{2A}^j} + F_{N_{1A}^j}F^*_{N_{2SN}^j}}_{(a)} + \underbrace{F_{N_{1SN}^j}F^*_{N_{2SN}^j}}_{(b)} + \underbrace{F_{N_{1A}^j}F^*_{N_{2A}^j}}_{(c)} \tag{23}$$

Shot noise and aerodynamic contributions are statistically independent; term (a) is thus zero if m is large enough, and the crossed term (b) is also null. Hence,

$$|P_{N1N2}(f)| \simeq \left|F_{N_{1A}^j}F^*_{N_{2A}^j}\right| \tag{24}$$

and the spectrum of density fluctuations is estimated by

$$\left|P_{\rho'^2}(f)\right| \simeq \frac{f_s^2}{k_1 k_2}\left|P_{N1N2}(f)\right| \tag{25}$$

An example of spectrum measured in the mixing layer of a Mach 0.9 cold jet is shown in Fig. 10. The frequency resolution is 800 Hz, and the noise floor is observed for frequencies higher than 100 kHz, but the dynamic could be extended by taking a larger m and reducing the frequency resolution. Beside, the phase plot indicates a near-zero lag for frequencies below 100 kHz, which confirms that the two collectors point toward the same probed volume. Furthermore, the frequency above which the phase becomes irregular is a good indicator of the maximum achievable frequency until the shot noise dominates.

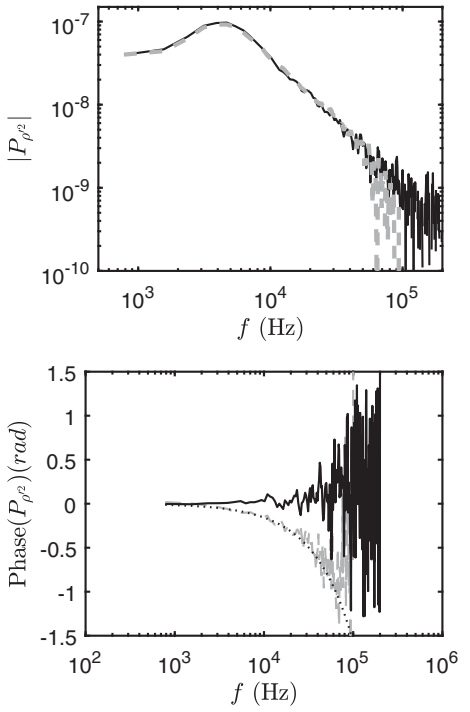

Fig. 10 Amplitude (top) and phase (bottom) of a measured spectrum of density fluctuations. —, two PMs; – – –, one PM; ⋯, phase lag Eq. (27).

The rms value of density fluctuations is finally determined from the Parseval identity:

$$\sigma^2_{\rho'} = \sum_{i=1}^{f_s/(2\Delta f)} \left|P_{\rho'^2}(i\Delta f)\right|\Delta f \tag{26}$$

3. *One-Photomultiplier Cross-Spectrum*

Considering only the contribution of the shot noise, all the consecutive samples of one given count rate signal constitute statistically independent realizations of shot noise. In opposition, density fluctuations are characterized by an integral time scale, and two measures separated by an interval of time smaller than this scale are closely related. By extension, if the time interval is much smaller than the turbulence time scale, the contribution of density fluctuations to the count rate would be very similar between two samples, and the contribution of shot noise remains random. This property allows to make two signals from the original that are related for density fluctuations but independent regarding shot noise. Considering a signal $N_d(t)$ with $t = 0, dt, 2dt, 3dt \ldots$, the first signal is made from the samples at $t = 2ndt$ with $n = 0, 1, 2, 3, \ldots$, and the second is made from the samples at $t = 2ndt + 1$. By doing so, two signals provided by two virtual sensors are obtained, except that the resulting sampling frequency is now divided by 2, and a frequency-dependent phase lag $\phi(f)$ associated with the time shift $1/f_s$ is introduced:

$$\phi(f) = \frac{-2\pi f}{f_s} \tag{27}$$

The spectra calculated either from two signals from one or two sensors are superimposed in Fig. 10. The comparison demonstrates well the ability of these two methods to provide very similar results until the noise floor is reached. Adjusting the sampling frequency and the frequency resolution permits dealing with most flows as long as they are governed by a self-similar behavior at high frequency to make possible the increase of Δf. The phase plot in Fig. 10 also shows that the result for one photomultiplier is consistent with the phase lag expected from Eq. (27).

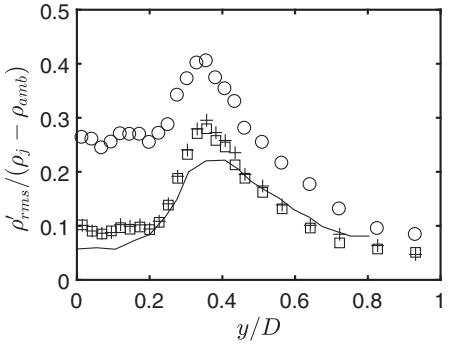

Fig. 11 Radial profile of density fluctuations at $z = 3D$. □ with two PMs; + with one PM; ○ from Eq. (20); — from Panda and Seasholtz [3].

4. Comparison of the Three Methods

Density fluctuations are finally computed from the three methods introduced previously, and the results are displayed in Fig. 11. The estimation derived from Eq. (20) is significantly larger than those computed from the cross-spectral method. This is directly related to the excess of fluctuations observed in Fig. 6 and confirms that this method should not be used in practice. Results obtained from Eq. (26), either from one or two sensors, are identical. The profile is also found similar with a profile from Panda and Seasholtz [3] measured at $z = 4D$ in a Mach 0.95 jet.

IV. Conclusions

A new processing is developed by means of the fast digitization of photomultiplier output signals. In comparison with the classical techniques, an increase of the maximum counted photon flux is achieved that benefits to the signal-to-noise ratio. Moreover, the sampling frequency of the photon count rate can be adjusted during postprocessing. It particularly serves the identification of spurious spikes due to dust passing across the probed volume, and their removal. Finally, density fluctuation spectra are considered using a single photomultiplier configuration, usually strongly affected by shot noise, and a two-photomultiplier configuration previously used to restrict the effect of shot noise but to the detriment of more difficult settings. An original data treatment applied in the single photomultiplier configuration helps to reduce shot noise effects in the spectrum estimation. This method is found as efficient as the two-photomultiplier configuration.

Acknowledgments

This work was performed within the framework of the Labex CeLyA of Université de Lyon, within the program "Investissements d'Avenir" (ANR-10-LABX-0060/ANR-11-IDEX-0007) operated by the French National Research Agency (ANR), and it is also partially supported by the industrial Chair ADOPSYS cofinanced by SAFRAN-SNECMA and ANR (ANR-13-CHIN-0001-01).

References

[1] Richards, C. D., and Pitts, W. M., "Global Density Effects on the Self-Preservation Behaviour of Turbulent Free Jets," *Journal of Fluid Mechanics*, Vol. 254, Sept. 1993, pp. 417–435. doi:10.1017/S0022112093002204

[2] Seasholtz, R. G., and Panda, J., "Multiple Point Dynamic Gas Density Measurements Using Molecular Rayleigh Scattering," *Proceedings of the 18th ICIASF*, IEEE Publ., Piscataway, NJ, 1999, pp. 43/1–43/10. doi:10.1109/ICIASF.1999.827183

[3] Panda, J., and Seasholtz, R. G., "Experimental Investigation of Density Fluctuations in High-Speed Jets and Correlation with Generated Noise," *Journal of Fluid Mechanics*, Vol. 450, Jan. 2002, pp. 97–130. doi:10.1017/S002211200100622X

[4] Panda, J., Seasholtz, R. G., and Elam, K. A., "Investigation of Noise Sources in High-Speed Jets Via Correlation Measurements," *Journal of Fluid Mechanics*, Vol. 537, Aug. 2005, pp. 349–385. doi:10.1017/S0022112005005148

[5] Panda, J., "Experimental Investigation of Turbulent Density Fluctuations and Noise Generation from Heated Jets," *Journal of Fluid Mechanics*, Vol. 591, Nov. 2007, pp. 73–96. doi:10.1017/S0022112007007173

[6] Panda, J., "A Molecular Rayleigh Scattering Setup to Measure Density Fluctuations in Thermal Boundary Layers," *Experiments in Fluids*, Vol. 57, No. 12, Nov. 2016, p. 183. doi:10.1007/s00348-016-2267-9

[7] Seasholtz, R. G., Panda, J., and Elam, K. A., "Rayleigh Scattering Diagnostic for Measurement of Velocity and Density Fluctuation Spectra," *44th AIAA Aerospace Sciences Meeting and Exhibit*, AIAA Paper 2002-0827, 2002. doi:10.2514/6.2006-837

[8] Mielke, A. F., and Elam, K. A., "Dynamic Measurement of Temperature, Velocity, and Density in Hot Jets Using Rayleigh Scattering," *Experiments in Fluids*, Vol. 47, Nos. 4–5, Oct. 2009, pp. 673–688. doi:10.1007/s00348-009-0708-4

[9] Mielke-Fagan, A. F., Clem, M. M., and Elam, K. A., "Rayleigh Scattering Measurements Using a Tunable Liquid Crystal Fabry-Perot Interferometer," *27th AIAA Aerodynamic Measurement Technology and Ground Testing Conference*, AIAA Paper 2010-4350, 2010. doi:10.2514/6.2010-4350

[10] Miles, R. B., Lempert, W. R., and Forkey, J. N., "Laser Rayleigh Scattering," *Measurement Science and Technology*, Vol. 12, No. 5, 2001, pp. R33–R51. doi:10.1088/0957-0233/12/5/201

[11] Young, A. T., "Rayleigh Scattering," *Physics Today*, Vol. 35, No. 1, Jan. 1982, pp. 42–48. doi:10.1063/1.2890003

[12] Panda, J., and Seasholtz, R. G., "Density Measurement in Underexpanded Supersonic Jets Using Rayleigh Scattering," *36th AIAA Aerospace Sciences Meeting and Exhibit*, AIAA Paper 1998-16178, 1998. doi:10.2514/6.1998-281

P. Givi
Associate Editor